Journal of Power Sources 327 (2016) 535–542

Contents lists available at ScienceDirect

Journal of Power Sources

journal homepage: www.elsevier.com/locate/jpowsour

Highly microporous carbons derived from a complex of glutamic acid and zinc chloride for use in supercapacitors

Xiao-Ling Dong, An-Hui Lu, Bin He, Wen-Cui Li*

State Key Laboratory of Fine Chemicals, School of Chemical Engineering, Dalian University of Technology, Dalian 116024, PR China

HIGHLIGHTS

- L-glutamic acid is a new carbon precursor with nitrogen functionality.
- Pyrolysis of a complex from L-glutamic acid and $ZnCl_2$ leads to carbon formation.
- Carbon is highly microporous due to the evaporation of zinc species.
- Carbon as electrode for EDLC possesses stable cycle life and low leakage current.

ARTICLE INFO

Article history:
Received 15 April 2016
Received in revised form
22 July 2016
Accepted 26 July 2016
Available online 30 July 2016

Keywords:
L-glutamic acid
Coordination
Microporous carbon
Nitrogen doping
Supercapacitors

ABSTRACT

The selection of carbon precursor is an important factor when designing carbon materials. In this study, a complex derived from L-glutamic acid and zinc chloride was used to prepare highly microporous carbons *via* facile pyrolysis. L-glutamic acid, a new carbon precursor with nitrogen functionality, coordinated with zinc chloride resulted in a homogeneous distribution of Zn^{2+} on the molecular level. During pyrolysis, the evaporation of the *in situ* formed zinc species creates an abundance of micropores together with the inert gases. The obtained carbons exhibit high specific surface area (S_{BET}: 1203 $m^2\ g^{-1}$) and a rich nitrogen content (4.52 wt%). In excess of 89% of the pore volume consists of micropores with pore size ranging from 0.5 to 1.2 nm. These carbons have been shown to be suitable for use as supercapacitor electrodes, and have been tested in 6 M KOH where a capacitance of 217 F g^{-1} was achieved at a current density of 0.5 A g^{-1}. A long cycling life of 30 000 cycles was achieved at a current density of 1 A g^{-1}, with only a 9% loss in capacity. The leakage current through a two-electrode device was measured as 2.3 μA per mg of electrode and the self-discharge characteristics were minimal.

1. Introduction

Supercapacitors (also referred to as electrical double layer capacitors – EDLCs), have attracted considerable interest due to their potential use in electrical vehicles, digital devices and pulsing techniques [1–3]. Due to the high electrical conductivity, ease of processability, controllable heteroatom doping, excellent electrochemical stability and good capacitive performance, porous carbons are regarded as first choice candidate electrode materials for supercapacitors which store energy *via* the accumulation of electrical charges across the electrode/electrolyte interface [4,5]. To date, various porous carbons including carbon spheres [6,7], carbon tubes [8], carbon fibers [9,10], carbon nanosheets [11,12] and graphene [13,14] have been studied as electrodes in supercapacitors. It has been generally accepted that micropores in these porous carbons are crucial sites for strengthening the electric double layer for high capacitance. The specific capacitance undergoes a sharp increase in carbons with pore sizes of <1 nm [15,16]. In addition, pores with sizes of 0.7–1.2 nm generate an optimum specific capacitance in aqueous electrolyte on account of the pore size being close to the desolvated electrolyte ions, thus leading to a maximum electrical double-layer capacitance [17–22]. However, supercapacitors based on microporous carbons are known to suffer from electrode kinetic problems that are related to the limitation of electrolyte ions penetrating the inner pores of electrodes [23]. To address this problem, one effective solution is to introduce heteroatoms into the microporous carbon skeleton, thus increasing the wettability of the electrode surface and the accessibility of the micropores [24,25]. The focus of the current work is

* Corresponding author.
E-mail address: wencuili@dlut.edu.cn (W.-C. Li).

http://dx.doi.org/10.1016/j.jpowsour.2016.07.100
0378-7753/

therefore to develop a synthesis approach for a microporous carbon integrating a narrow micropore size distribution and heteroatom modification in order to simultaneously achieve properties of a high capacitance, good rate performance and long cycle life.

To achieve this goal, herein we propose the use of L-glutamic acid as a new and single carbon precursor. L-glutamic acid, which contains abundant functional groups such as -NH_2 and -COOH, has a strong tendency to coordinate with inorganic cations, e.g. Zn^{2+}. The advantage of using L-glutamic acid as a carbon precursor therefore is that the zinc cations can be homogeneously distributed on a molecular level. The synthesized carbon materials are expected to possess abundant micropores from the evaporation of the in situ-formed and uniformly dispersed Zn species during the carbonization process [26,27]. When such microporous carbons are used as supercapacitor electrodes, they show an excellent capacitive performance. It is anticipated that this synthesis can be relatively easily scaled up to an industrial level.

2. Experimental section

2.1. Chemicals

L-glutamic acid (99%) was purchased from J&K Scientific Ltd. Zinc chloride (98%) was purchased from Sinopharm Chemical Reagent Co., Ltd. All chemicals were used as received without further purification.

2.2. Synthesis of microporous carbons

In a typical synthesis procedure, L-glutamic acid was first dissolved in water to form a clear solution with vigorous stirring at 60 °C. Afterwards, zinc chloride dispersion was added to the above solution and stirred until the reaction solution was again homogeneous. Subsequently, the water in the homogeneous solution was removed by reduced pressure distillation and the obtained compound was transferred to an oven at 90 °C for 12 h followed by pyrolysis at 910 °C (the evaporation temperature of metal Zinc) for 2 h under an argon atmosphere to obtain porous carbon. By varying the molar ratio of zinc chloride to L-glutamic acid (2:1, 1:1 and 0.5:1), three samples (denoted as Glu-Zn-2, Glu-Zn-1 and Glu-Zn-0.5) with different pore volumes were prepared. As a control experiment, one sample (denoted as Glu-Zn-0) was also prepared by direct pyrolysis of L-glutamic acid at 910 °C in an argon atmosphere.

2.3. Structure characterization

Scanning electron microscopy (SEM) images were obtained on a Hitachi S-4800 instrument. Transmission electron microscopy (TEM) images were recorded on a FEI Technai F30 equipment operating at 200 kV. The samples for TEM analysis were prepared by placing a droplet of the products in EtOH onto carbon-coated copper grids and drying at room temperature. The X-ray diffraction (XRD) patterns were obtained on a Rigaku D/Max 2400 diffractometer by using CuKα radiation (40 kV, 100 mA, $\lambda = 1.5406$ Å). The specific surface area and porous structure were determined by nitrogen sorption on a Micromeritics ASAP 2020 device at 77 K, and prior to analysis, all samples were degassed under a pressure of 0.05 mbar at 200 °C for 12 h. The Brunauer-Emmett-Teller (BET) method was used to calculate the specific surface areas (S_{BET}). Total pore volumes (V_{total}) were calculated from the amount of nitrogen adsorbed at a relative pressure, P/P_0 of 0.99. The pore size distribution was obtained using the Non-Local Density Functional Theory (NLDFT) method. Elemental analysis was carried out on a CHNO elemental analyzer (Vario EL III, Elementar). The weight ratio of zinc was determined through inductively coupled plasma optical emission spectrometry (ICPOES, Perkin Elmer, Optima 2000 DV ICP-OES). X-ray photoelectron spectroscopy (XPS) data were obtained with an ESCALAB250 electron spectrometer.

2.4. Electrochemical measurements

The working electrodes were prepared by mixing porous carbons, Ketjen Black and polytetrafluoroethylene (PTFE) binder with weight ratio of 8:1:1. The slurry of the mixture was rolled into a film, cut into suitable shapes and placed into an oven at 90 °C for 10 h, followed by placing it on a foam nickel current collector with an area of 1 cm^2 under a pressure of 10 MPa to fabricate an electrode. The mass loading of the active material was approximately 4 mg cm^{-2}. The capacitive performance of the single electrode was carried out on an CHI660D electrochemical workstation (CH Instruments Inc., Shanghai, China) using a standard three-electrode test system composed of Hg/HgO as a reference electrode and a Pt plate as a counter electrode in 6 M KOH electrolyte at 25 °C. Cyclic voltammetry (CV) and galvanostatic charge-discharge cycling (GC) measurements were employed in the evaluation of the electrode electrochemical performance. Electrochemical impedance spectroscopy measurements were carried out in the range of 0.01 Hz–100 kHz with ac amplitude of 5 mV. The specific gravimetric capacitance based on the GC test was calculated using the following equation: $C = I\Delta t/m\Delta V$, where I (A), t (s), ΔV (V) and m (g) are the discharge current, the discharge time, the voltage window from the end of the internal resistance (IR) drop to the end of the discharge process, and the mass of active material, respectively. The cycle life, leakage current and self-discharging performances were measured by a multichannel electrochemical workstation (Arbin Instruments USA).

3. Results and discussion

To synthesize desired microporous carbons, the selection of carbon precursor is crucial. In this study, we use L-glutamic acid as a single carbon precursor based on the consideration that it contains abundant functional groups such as -NH_2 and -COOH, and has a strong tendency to coordinate with zinc cations. The FTIR spectrum of the as-prepared carbon precursor in Fig. S1 is evidence that the L-glutamic acid can indeed coordinate with Zn^{2+}. Moreover, Zn^{2+} can combine with the lone pair electrons of the nitrogen atom in nitrogen-containing ligands such as -NH_2 [28]. This in turn facilitates the immobilization of the nitrogen atoms in the carbon framework. Based on the above, we used L-glutamic acid and $ZnCl_2$ as the starting materials, with the expectation that the highly dispersed Zn cations would act as facile porogens by volatilization of *in situ* formed Zn clusters and thus lead to the formation of an abundance of micropores [27].

By varying the molar ratio of zinc chloride to L-glutamic acid (2:1, 1:1 and 0.5:1), three carbon samples were prepared with a carbonization yields of ca. 19 wt% (910 °C). The synthesized carbon materials were characterized by TEM, to gain an insight into the microstructures. Since the structures of all the samples are very similar from TEM observations, representative TEM images of Glu-Zn-2 are shown in Fig. 1a and b. It can be seen that the carbon skeleton of Glu-Zn-2 is highly amorphous and homogeneous in absence of visible Zn clusters. To check the homogeneity of the Zn^{2+} distribution in the carbon precursor, the carbon product derived from the Glu-Zn-2 precursor carbonized at 600 °C (denoted as Glu-Zn-2-600) was characterized using Energy-dispersive X-ray spectroscopy (EDX). As shown in Fig. S2, the element mappings of the representative regions show a concordance of the Zn, C, and O

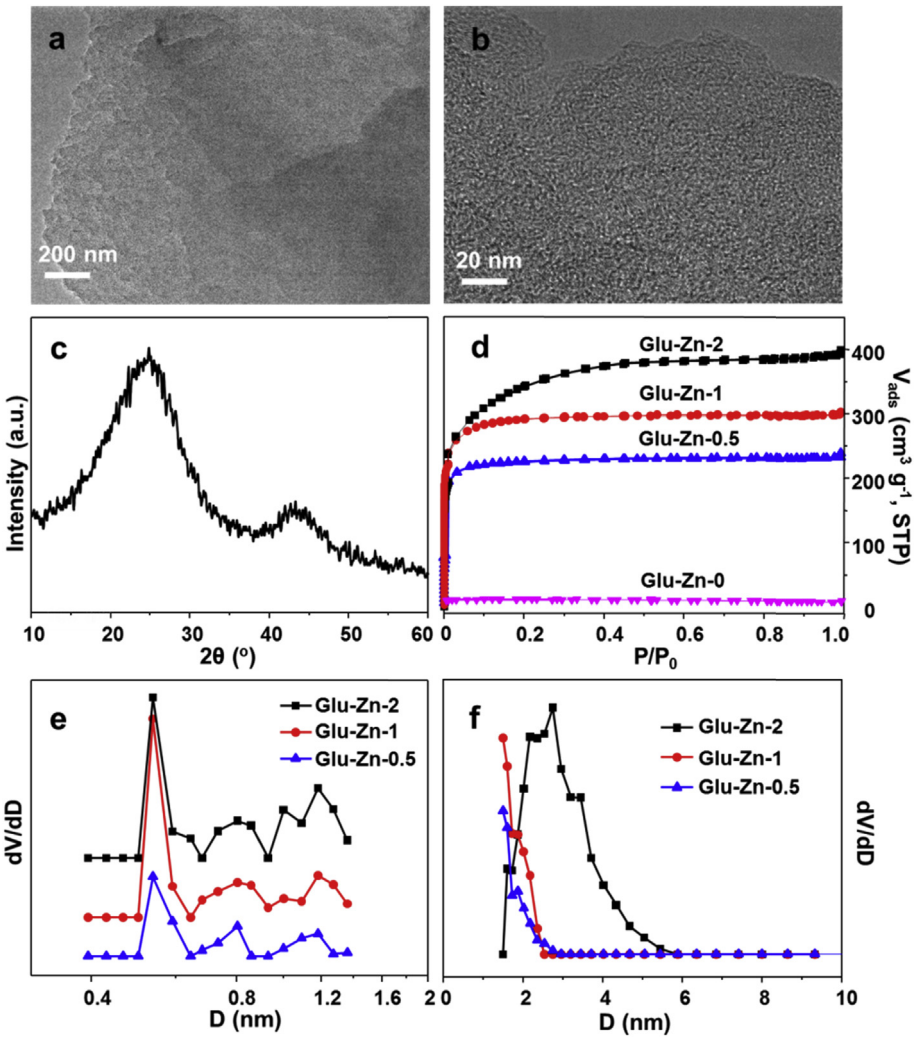

Fig. 1. (a, b)TEM images of Glu-Zn-2. (c) XRD pattern of Glu-Zn-2 (d) Nitrogen sorption isotherms of Glu-Zn-2, Glu-Zn-1, Glu-Zn-0.5 and Glu-Zn-0 (e) Micropore and (f) Mesopore size distribution of the samples prepared with different weight ratios of $ZnCl_2$.

signals, suggesting the existence and uniform distribution of Zn and O elements. On the basis of the EDX results, we conclude that the molecular porogens are uniformly dispersed in the carbon precursor. The XRD pattern included in Fig. 1c also confirms the amorphous structure of the carbon materials in which broad and low-intensity (002) and (10) bands can be identified. Moreover, no detectable peaks corresponding to Zn species are found on the XRD of carbon samples calcined at 910 °C, indicating that Zn species were released from the carbon matrix during the carbonization process. This conclusion is in agreement with the 0.02% weight ratio of Zn in Glu-Zn-2 determined through inductively coupled plasma optical emission spectrometry (ICP-OES).

Nitrogen physisorption measurements were carried out to gain further insight into the porosities of the carbons. The N_2 sorption isotherms of the samples are shown in Fig. 1d. It can be seen that the curves for all the samples exhibit typical type I isotherms with sharp uptake at low relative pressure ($P/P_0 < 0.05$), which indicate they are microporous. Fig. 1e shows the pore size distributions determined using the DFT method, in which distributions of micropores 0.5–1.2 nm in size are evident for all the carbons. This narrow distribution of micropores further confirms the homogeneous pore formation created by the zinc species. For Glu-Zn-2, a small number of mesopores with pore diameter ranging from 2 to 5 nm was also observed (Fig. 1f), which may be attributed to the evaporation of aggregated residual Zn that was not coordinated with L-glutamic acid when using the higher $ZnCl_2$ dosage. The surface areas and pore volume of all samples measured with N_2 sorption analysis are shown in Table 1. It can be seen that Glu-Zn-0 prepared without the use of zinc precursor as the porogen, has the lowest specific surface area of 39 $m^2\ g^{-1}$, while the surface areas of the carbon samples using zinc precursor as the porogen increase steadily to 761, 989 and 1203 $m^2\ g^{-1}$ for samples Glu-Zn-0.5,Glu-Zn-1 and Glu-Zn-2 respectively. This shows that the higher the amount of zinc precursor used, the higher the S_{BET} of the resulting carbon materials.

The surface properties of a carbon electrode play an important role in the electrochemical performance, as they can influence the

Table 1
Structure parameters of the glutamic acid derived microporous carbons.

Samples	S_{BET}/$m^2\ g^{-1}$	V_{total}/$cm^3\ g^{-1}$	V_{micro}/$cm^3\ g^{-1}$
Glu-Zn-2	1203	0.62	0.55
Glu-Zn-1	989	0.47	0.45
Glu-Zn-0.5	761	0.37	0.35
Glu-Zn-0	39	0.023	0.01

wettability of the electrolyte on the carbon electrode. Thus, the surface and bulk composition of the samples were analyzed by XPS and elemental analysis. The chemical compositions of the obtained carbon materials are shown in Table 2. It can be seen that a relatively high amount of nitrogen (2.59–6.06 wt%) and oxygen (6.35–17.34 wt%) species are present in the samples, derived from the intrinsic nitrogen and oxygen in the L-glutamic acid. The presence of nitrogen and oxygen groups on the carbon surface are considered to enhance the wettability of the carbon materials, facilitate the accessibility of the electrolyte ions, and give rise to Faradaic pseudocapacitive reactions [21,24,25]. It can be seen that the content of bulk nitrogen (6.06 wt%) in Glu-Zn-0 is higher than that of the samples prepared using the zinc porogen. This is possibly due to its low porosity, thus restricting the evaporation of the nitrogen, *i.e.*, a high surface area indicates more open pores allowing the easy escape of nitrogen atoms from the substrate. Among the samples prepared using zinc porogen, a trend can be seen of increasing nitrogen content with an increase in the amount of zinc porogen that is associated with a more developed pore structure. This is related to the enhanced interaction between zinc cations and the lone pair electrons in nitrogen and the subsequent immobilization of the nitrogen in the carbon framework.

The percent of doped nitrogen was estimated by XPS analysis to be 3.38, 2.99 and 1.78 atom% for Glu-Zn-2, Glu-Zn-1 and Glu-Zn-0.5 respectively. These values are slightly lower than the bulk nitrogen values from the elemental analysis. The full scan XPS curves of the four samples (Fig. S3) have three peaks centered at binding energies of *ca.* 284.6, 398.2 and 531.9 eV, corresponding to C 1s, N 1s and O 1s respectively. Fig. 2 shows the N 1s spectra of the samples, which can be fit to four peaks with binding energies of 398.0 ± 0.2 eV, 399.7 ± 0.2 eV, 400.8 ± 0.2 eV and 402.5 ± 0.2 eV and assigned to pyridinic N (N-6), pyrrolic or pyridonic N (N-5), quaternary N (N-Q) and oxidized N (N-X), respectively. These have all been proven to be active in supercapacitors [29–33]. The contribution of each species obtained by fitting the N1s core level spectra for all samples studied are listed in Table 2. As shown in previous studies, N-6 and N-5 are considered to enhance the electron donor/acceptor properties in an alkaline aqueous solution and further improve the pseudo-capacitance [30]. The N atom substituents N-Q within the carbon layers and N-X can enhance the electronic conductivity of carbon materials [31–33].

The high surface areas, abundant micropores and nitrogen doping make the glutamic acid derived carbon materials ideal candidates for use as electrodes for supercapacitors. Thus, a three-electrode system in 6 M KOH was used to characterize the capacitive properties of the obtained carbons. As indicated in Fig. 3a, the cyclic voltammograms of the three samples show approximately rectangular-like shapes with -broadened redox peaks at lower potential, indicating the possible coexistence of double layer capacitance and pseudocapacitance due to redox reaction of N atoms [34]. Additionally, electrochemically active nitrogen atoms could easily control local electronic structures, which contribute to enhance the band between the electrolyte ions of K^+ and the N atoms in the solution, resulting in plentiful K^+ ions accommodated on the electrode surface. Meanwhile the larger number of H_2O around the K^+ ions is also brought to the electrode surface [35]. It is noted that sample Glu-Zn-2 demonstrates a larger capacitive response than Glu-Zn-1 and Glu-Zn-0.5. This is further confirmed by the triangular-shaped galvanostatic charge/discharge cycling curves shown in Fig. 3b. Unsurprisingly, the time of accomplishing a charge/discharge cycle is longer for Glu-Zn-2 than that for Glu-Zn-1 and Glu-Zn-0.5. The calculated mass capacitance (C_g) of Glu-Zn-2 reaches 217 F g^{-1} at a current density of 0.5 A g^{-1}, which is close to the previously reported supercapacitance of graphene film [36], B-/N-porous carbon [25] and N-doped carbon fiber [37], but superior to that of hierarchical nitrogen-doped porous carbon [38] carbon nanosheets [39] and ordered mesoporous carbon/graphene aerogel [40].

Electrochemical impedance spectroscopy (EIS) was used to gain an insight into the kinetic behaviors of the samples for supercapacitance. In Fig. 3c, all three electrodes show a similar Nyquist plot shape with, at the high frequency region a depressed semicircle on the Z'axis, and at the low-frequency region an approximately straight line parallel to the Z″ axis. These shapes indicate ideal capacitive behavior. The Nyquist curves were fit using the equivalent circuit illustrated in Fig. 3 (the inset in the upper right). In this circuit, Rs represents the combined resistance involving intrinsic resistance of substrate, ionic resistance of electrolyte and the contact resistance at the active material-current collector interface. Rct is the charge transfer resistance, which is caused by the faradic interactions between the nitrogen species on the materials and ion in solution and the double-layer capacitance at the electrode electrolyte interface. Zw is associated with the Warburg impedance. CPE represents the capacitance inside the pores. All fitted results are shown in Table S1. On the basis of the same testing conditions, Glu-Zn-2 has the lowest Rs (0.43 Ω), better than that of Glu-Zn-1 and Glu-Zn-0.5. This may be ascribed to the enhanced electrical conductivity resulting from its higher N content [31–33]. The charge transfer resistances of electrodes Glu-Zn-1 and Glu-Zn-2 (0.08 Ω) are lower than that of Glu-Zn-0.5 (0.15 Ω), possibly due to their higher nitrogen doping that quaternary N and oxidized N species possibly due to their higher quaternary N and oxidized N species, on which the positive charge helps in electron transport through the carbon materials [31–33]. Additionally, their higher nitrogen doping results in better wetting on them, which lowers the transfer resistance by increasing the effective contact area [41]. In the low frequency region, the Glu-Zn-2 electrode shows a smaller Zw (0.17 Ω) denoted by a sharp line, which is a result of the presence of some mesopores giving improved electrolyte diffusion efficiency. For the Glu-Zn-2 electrode, the relatively low values of Rs, Rct and Zw indicate higher diffusion and migration pathways for electrolyte ions during charge/discharge processes which are responsible for the superior electrochemical performance of supercapacitors.

Table 2
Elemental analysis of the carbon samples.

Samples	Elemental analysis[a] (wt%)				XPS[c] (atom%)			Relative surface contents of nitrogen			
	C	H	N	O[b]	C	N	O	N-6	N-5	N-Q	N-X
Glu-Zn-2	79.03	1.67	4.52	14.79	91.05	3.38	5.57	28.6	28.1	35.4	7.9
Glu-Zn-1	77.46	1.32	3.88	17.34	92.05	2.99	4.96	29.6	13.9	38.7	17.8
Glu-Zn-0.5	86.06	0.90	2.59	10.45	93.31	1.78	4.91	17.2	22.3	37.9	22.6
Glu-Zn-0	83.72	0.85	6.06	6.35	86.14	1.99	11.87	15.9	44.8	21.6	17.7

[a] The C, H, N contents were directly measured by elemental analysis.
[b] Calculated by difference.
[c] Weight percentage of C, N and O elements obtained from XPS analysis.

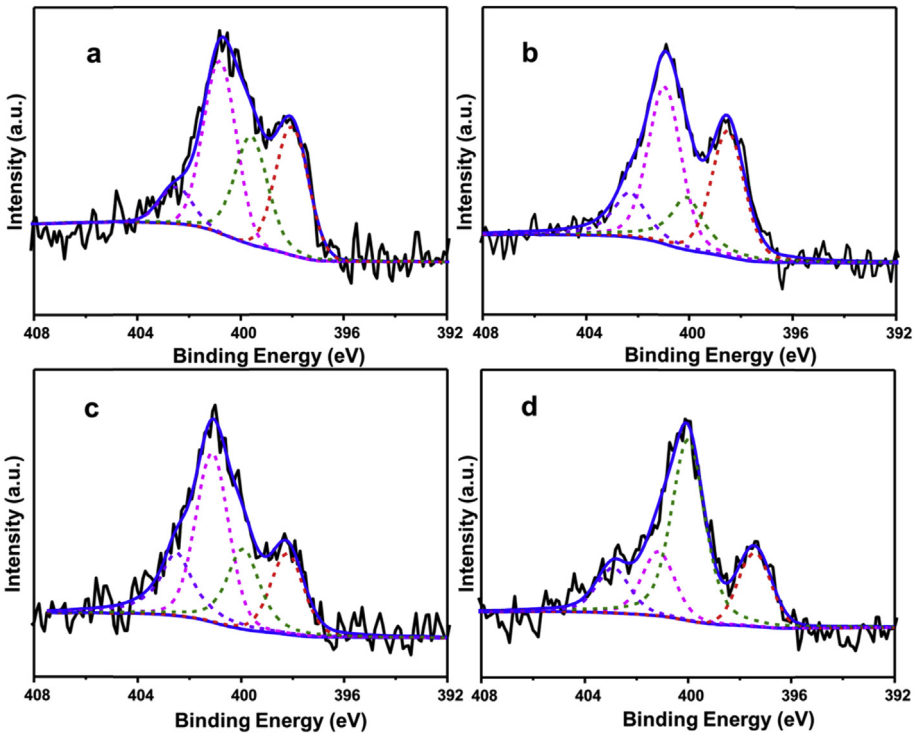

Fig. 2. XPS N 1s spectra of (a) Glu-Zn-2, (b) Glu-Zn-1, (c) Glu-Zn-0.5 and (d) Glu-Zn-0.

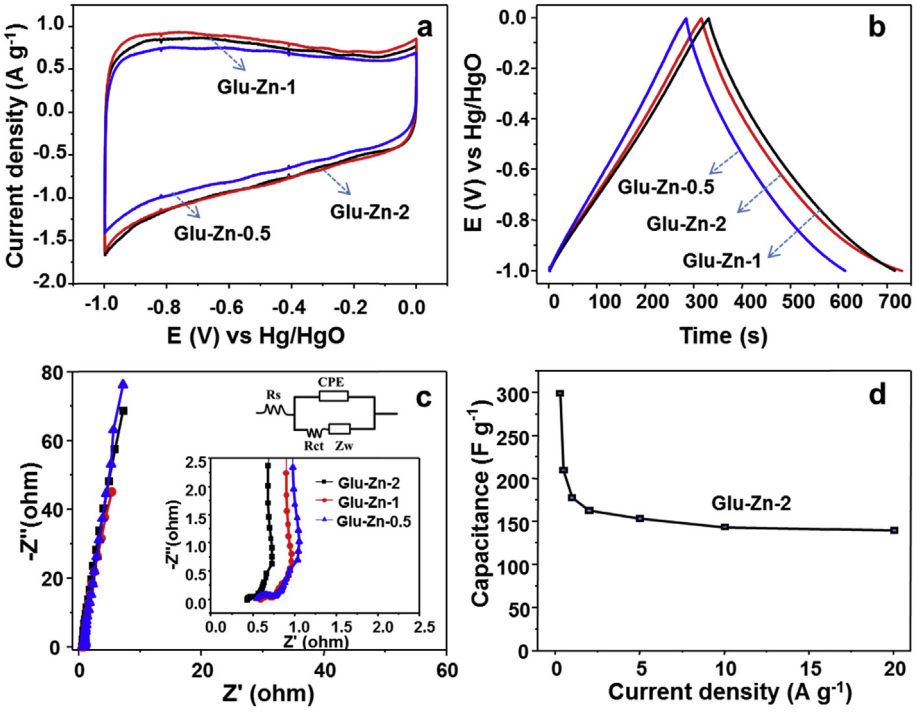

Fig. 3. Electrochemical performance of the synthesized microporous carbons Glu-Zn-2, Glu-Zn-1 and Glu-Zn-0.5 (a) CVs measured at 5 mV s^{-1} and (b) GC curves measured at 0.5 A g^{-1} of samples. (c) Nyquist plots in the frequency range of 100 kHz to 10 mHz in KOH electrolyte at 25 °C (d) The specific capacitance of Glu-Zn-2 at different current densities (0.3–20 A g^{-1}).

The enhanced capacitive performance of Glu-Zn-2 can possibly be correlated to the combined effect of the carbon texture characteristics and surface functionalities. First, Glu-Zn-2 has the similar micropore size distribution to the other two samples, but has a largest surface area, which is necessary to provide an electrode/electrolyte interface for the formation of electrostatic charge-separation layers in the pores. Moreover, the existence of some amount of mesopores in Glu-Zn-2 is beneficial to the diffusion of

ions. Second, the highly doped nitrogen in Glu-Zn-2 will contribute to pseudocapacitive charge storage and electron conductivity. It has been reported that N-5 and N-6 groups are primarily responsible for the pseudocapacitive charge storage *via* the redox reaction of the negatively charged surface groups (N-5 and N-6), while N-Q and N-X groups aid electron transfer through their positive charge [30–33]. The fitted impedance data also indicates a high conductivity of the Glu-Zn-2 electrode. Thus the higher doped N content (4.52 wt%) in Glu-Zn-2 plays an important role in boosting the capacitive performance.

Rate capability is an important factor for the utilization of supercapacitors in power applications. A good electrochemical energy storage device is required to provide high energy density (or gravimetric capacitance) at a high charge/discharge rate. CV tests at different scan rates and GC tests at different current densities for the representative samples are shown in Fig. S4. It can be seen that when the scan rate gradually increases from 5 to 200 mV s^{-1}, the rectangular shape is retained (Fig. S4a), indicating a good capacitance performance at a high scan rate. Moreover, all GC curves show symmetrical triangular shapes, exhibiting only a small IR drop at a high current density (Fig. S4b), implying that the supercapacitor has a high reversibility of a typical capacitor with a rapid I-V response and a small equivalent series resistance. This is in accordance with the result of EIS. The variation of specific capacitances at different current densities for Glu-Zn-2 is summarized in Fig. 3d. Glu-Zn-2 exhibits a high rate capability of 160 F g^{-1} at a current density as high as 20 A g^{-1}. A high capacitance retention ratio of 73.7% is observed at current densities from 0.5 to 20 A g^{-1}. These results indicate a very fast and efficient charge transfer and high capacitance of the Glu-Zn-2 electrode which is maintained under high current densites. It can therefore be concluded that such microporous carbons facilitate the efficient access of electrolytes with the surface wettability and electronic conductivity required for a high specific capacitance.

The cycling stability of Glu-Zn-2 was examined using galvanostatic charge/discharge cycling at a current density of 1 A g^{-1} for 30,000 cycles (Fig. 4a) in a symmetrical two-electrode system. A capacitance retention of 90% (44 F g^{-1}) was obtained after 30,000 cycles, indicating an excellent performance stability of the microporous carbons. The GC curves of the last 5 cycles (Fig. 4c) retained an almost identical shape to the first 5 cycles (Fig. 4b) by maintaining their linearity and symmetry. This further reveals that the Glu-Zn-2 electrode has a good electrochemical capacitance and excellent long-term cycle stability.

For practical applications, it is important to evaluate the leakage current and self-discharge characteristics of the assembled supercapacitors. These are typically not discussed in the literature. Our Glu-Zn-2 based two-electrode symmetrical supercapacitor was first charged to 1.0 V at 0.5 A g^{-1}, and then the potential was maintained at 1.0 V for 4 h and the current flowing through the supercapacitor was recorded. In this constant voltage mode, the current through the stabilized device compensates the current loss by the capacitor itself, which can be viewed as the leakage current. For the supercapacitor assembled from the glutamic acid derived microporous carbon, the current quickly stabilizes at 15.7 μA, which is essentially the leakage current through the device (Fig. 4d). This value (2.3 μA per mg electrode) is comparable to those of a carbon nanotube/polyaniline composite supercapacitor (17.2 μA, 5.5 μA per mg electrode) [42], hierarchically porous carbons based supercapacitor (0.04 mA) [43] and polyaniline-coated carbon paper based supercapacitor (16 μA) [44], indicating a relatively small leakage current and high stability of our supercapacitor. A lower leakage current implies a higher leakage resistance that ensures slow self-discharge phenomenon of supercapacitors [45]. The stability of the device and its capability for retaining charges were further demonstrated by a self-discharge test represented by the time course of the open-circuit voltage. As shown in Fig. 4e, the device after being charged at 1.0 V underwent a rapid self-discharge process in the first half hour and then slowed down after several hours. Finally the output voltage of the device reached

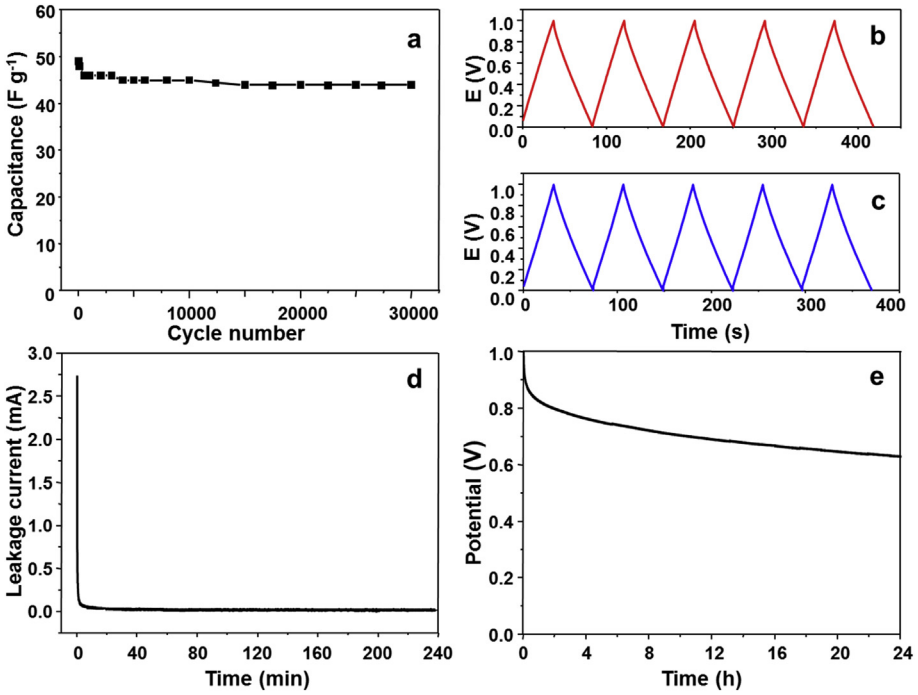

Fig. 4. (a) Cycle performance of the assembled supercapacitor based on Glu-Zn-2 at the current density of 1.0 A g^{-1} upon 30 000 cycles. (b, c) the first and last 5 cycles of GC curves. (d) Leakage current curve of the supercapacitor charged at 0.5 A g^{-1} to a floating potential of 1 V and kept at 1 V for 4 h. (e) Self-discharge curve after charge at 1 V for 24 h.

approximately 0.63 V after 24 h. These studies demonstrate that our devices exhibit low self-discharge characteristics, which is highly desirable in practical applications.

4. Conclusions

By using L-glutamic acid as new and single carbon precursor, highly microporous carbons have been synthesized *via* facile pyrolysis of a complex derived from L-glutamic acid and zinc chloride. By simply adjusting the ratio of L-glutamic acid to $ZnCl_2$, carbon with high specific surface area and an abundance of micropores can easily be prepared. During the preparation process, the in situ-formed and uniformly dispersed Zn species acting as molecular porogens evaporate to form these micropores. The obtained porous materials possess excellent capacitive performance as electrodes of supercapacitors, due predominantly to a narrow micropore distribution and N doping. Moreover, the unique properties and the potential scalable synthesis make these novel microporous carbons suitable for many other applications, such as sorbents and catalyst supports.

Acknowledgements

This work was supported by National Program on Key Basic Research Project (No.2013CB934104) and National Natural Science Foundation of China (No. 21376047, U1303192).

Appendix A. Supplementary data

Supplementary data related to this article can be found at http://dx.doi.org/10.1016/j.jpowsour.2016.07.100.

References

[1] R. Kötz, M. Carlen, Principles and applications of electrochemical capacitors, Electrochim. Acta 45 (2000) 2483–2498.
[2] J.R. Miller, P. Simon, Electrochemical capacitors for energy management, Science 321 (2008) 651–652.
[3] P. Simon, Y. Gogotsi, Materials for electrochemical capacitors, Nat. Mater. 7 (2008) 845–854.
[4] F. Beguin, V. Presser, A. Balducci, E. Frackowiak, Carbons and electrolytes for advanced supercapacitors, Adv. Mater. 26 (2014) 2219–2251.
[5] J. Yan, Q. Wang, T. Wei, Z. Fan, Recent advances in design and fabrication of electrochemical supercapacitors with high energy densities, Adv. Energy Mater. 4 (2014) 1300816–1300859.
[6] X.H. Xia, Y.Q. Zhang, Z.X. Fan, D.L. Chao, Q.Q. Xiong, J.P. Tu, H. Zhang, H.J. Fan, Novel metal @carbon spheres core shell arrays by controlled self-assembly carbon flexible supercapacitor, Adv. Energy Mater. 5 (2015), http://dx.doi.org/10.1002/aenm.201401709.
[7] S.K. Kim, E. Jung, M.D. Goodman, K.S. Schweizer, N. Tatsuda, K. Yano, P.V. Braun, Self-assembly of monodisperse starburst carbon spheres into hierarchically organized nanostructured supercapacitor electrodes, ACS Appl. Mater. Interfaces 7 (2015) 9128–9133.
[8] G. Sun, X. Zhang, R. Lin, J. Yang, H.C. Zhang, P. Hen, Hybrid fibers made of molybdenum disulfide, reduced graphene oxide, and multi-walled carbon nanotubes for solid-state, flexible, asymmetric supercapacitors, Angew. Chem. Int. Ed. 54 (2015) 4651–4656.
[9] X.Q. Zhang, Q. Sun, W. Dong, D. Li, A.H. Lu, J.Q. Mu, W.C. Li, Synthesis of superior carbon nanofibers with large aspect ratio and tunable porosity for electrochemical energy storage, J. Mater. Chem. A 1 (2013) 9449–9455.
[10] C. Kim, K.S. Yang, M. Kojima, K. Yoshida, Y.J. Kim, Y.A. Kim, M. Endo, Fabrication of electrospinning-derived carbon nanofiber webs for the anode material of lithium-ion secondary batteries, Adv. Funct. Mater. 16 (2006) 2393–2397.
[11] G.P. Hao, A.H. Lu, W. Dong, Z.Y. Ji, X.Q. Zhang, J.T. Zhang, W.C. Li, Sandwich-type microporous carbon nanosheets for enhanced supercapacitor performance, Adv. Energy Mater. 3 (2013) 1421–1427.
[12] Z.Y. Jin, A.H. Lu, Y.Y. Xu, J.T. Zhang, W.C. Li, Ionic liquid-assisted synthesis of microporous carbon nanosheets for use in high rate and long cycle life supercapacitors, Adv. Mater. 26 (2014) 3700–3705.
[13] T. Wang, L.X. Wang, D.L. Wu, W. Xia, D.Z. Jia, Interaction between nitrogen and sulfur in co-doped graphene and synergetic effect in supercapacitor, Sci. Rep. 5 (2015) 9591–9599.
[14] F. Xiao, S. Yang, Z. Zhang, H. Liu, J. Xiao, L. Wan, J. Luo, S. Wang, Y. Liu, Scalable synthesis of freestanding sandwich-structured graphene/polyaniline/graphene nanocomposite paper for flexible all-solid-state supercapacitor, Sci. Rep. 5 (2015) 9359–9366.
[15] J. Chmiola, G. Yushin, Y. Gogotsi, C. Portet, P. Simon, P.L. Taberna, Anomalous increase in carbon capacitance at pore sizes less than 1 nanometer, Science 313 (2006) 1760–1763.
[16] E. Raymundo-Pinero, K. Kierzek, J. Machnikowski, F. Beguin, Relationship between the nanoporous texture of activated carbons and their capacitance properties in different electrolytes, Carbon 44 (2006) 2498–2507.
[17] J. Chmiola, G. Yushin, R. Dash, Y. Gogotsi, Effect of pore size and surface area of carbide derived carbons on specific capacitance, J. Power Sources 158 (2006) 765–772.
[18] C. Lin, J.A. Ritter, B.N. Popov, Correlation of double-layer capacitance with the pore structure of sol-gel derived carbon xerogels, J. Electrochem. Soc. 146 (1999) 3639–3643.
[19] J. Chmiola, C. Largeot, P.L. Taberna, P. Simon, Y. Gogotsi, Desolvation of ions in subnanometer pores and its effect on capacitance and double-layer theory, Angew. Chem. Int. Ed. 120 (2008) 3440–3443.
[20] A.G. Pandolfo, A.F. Hollenkamp, Carbon properties and their role in supercapacitors, J. Power Sources 157 (2006) 11–27.
[21] C. Ma, Y. Song, J.L. Shi, D.Q. Zhang, X.L. Zhai, M. Zhong, Q. Guo, L. Liu, Preparation and one-step activation of microporous carbon nanofibers for use as supercapacitor electrodes, Carbon 51 (2013) 290–300.
[22] C. Largeot, C. Portet, J. Chmiola, P.L. Taberna, Y. Gogotsi, P. Simon, Relation between the ion size and pore size for an electric double-layer capacitor, J. Am. Chem. Soc. 130 (2008) 2730–2731.
[23] D. Qu, H. Shi, Studies of activated carbons used in double-layer capacitors, J. Power Sources 74 (1998) 99–107.
[24] J. Wei, D. Zhou, Z. Sun, Y. Deng, Y. Xia, D. Zhao, A controllable synthesis of rich nitrogen-doped ordered mesoporous carbon for CO_2 capture and supercapacitors, Adv. Funct. Mater. 23 (2012) 2322–2328.
[25] D.C. Guo, J. Mi, G.P. Hao, W. Dong, G. Xiong, W.C. Li, A.H. Lu, Ionic liquid $C_{16}mimBF_4$ assisted synthesis of poly(benzoxazine-co-resol)-based hierarchically porous carbons with superior performance in supercapacitors, Energy Environ. Sci. 6 (2013) 652–659.
[26] D. Qian, C. Lei, E.M. Wang, W.C. Li, A.H. Lu, A method for creating microporous carbon materials with excellent CO_2-adsorption capacity and selectivity, ChemSusChem 7 (2014) 291–298.
[27] F. Cheng, W.C. Li, J.N. Zhu, W.P. Zhang, A.H. Lu, Designed synthesis of nitrogen-rich carbon wrapped Sn nanoparticles hybrid anode via in-situ growth of crystalline ZIF-8 on a binary metal oxide, Nano Energy 19 (2016) 486–494.
[28] F.A. Brede, K. Mandel, M. Schneider, G. Sextlbc, K. Müller-Buschbaum, Mechanochemical surface functionalisation of superparamagnetic microparticles with in situ formed crystalline metal-complexes: a fast novel core-shell particle formation method, Chem. Commun. 51 (2015) 8687–8690.
[29] C.O. Ania, V. Khomenko, E. Raymundo-Pinero, J.B. Parra, F. Beguin, The large electrochemical capacitance of microporous doped carbon obtained by using a zeolite template, Adv. Funct. Mater. 17 (2007) 1828–1836.
[30] Z. Wen, X. Wang, S. Mao, Z. Bo, H. Kim, S. Cui, G. Lu, X. Feng, J. Chen, Crumpled nitrogen-doped graphene nanosheets with ultrahigh pore volume for high-performance Supercapacitor, Adv. Mater. 24 (2012) 5610–5616.
[31] Z. Li, Z. Xu, X. Tan, H. Wang, C. Holt, T. Stephenson, B.C. Olsen, D. Mitlin, Mesoporous nitrogen-rich carbons derived from protein for ultra-high capacity battery anodes and supercapacitors, Energy Environ. Sci. 6 (2013) 871–878.
[32] J. Hou, C. Cao, F. Idrees, X.L. Ma, Hierarchical porous nitrogen-doped carbon nanosheets derived from silk for ultrahigh-capacity battery anodes and supercapacitors, ACS Nano 9 (2015) 2556–2564.
[33] D. Hulicova-Jurcakova, M. Seredych, G.Q. Lu, T.J. Bandosz, Combined effect of nitrogen- and oxygen-containing functional groups of microporous activated carbon on its electrochemical performance in supercapacitors, Adv. Funct. Mater. 19 (2009) 438–447.
[34] B. Xu, S. Hou, G. Cao, F. Wu, Y. Yang, Sustainable nitrogen-doped porous carbon with high surface areas prepared from gelatin for supercapacitors, J. Mater. Chem. 22 (2012) 19088–19093.
[35] L. Sun, L. Wang, C. Tian, T. Tan, Y. Xie, K. Shi, M. Li, H. Fu, Nitrogen-doped graphene with high nitrogen level via a one-step hydrothermal reaction of graphene oxide with urea for superior capacitive energy storage, RSC Adv. 2 (2012) 4498–4506.
[36] Z. Lei, L. Lu, X.S. Zhao, The electrocapacitive properties of graphene oxide reduced by urea, Energy Environ. Sci. 5 (2012) 6391–6399.
[37] L.F. Chen, X.D. Zhang, H.W. Liang, M. Kong, Q.F. Guan, P. Chen, Z.Y. Wu, S.H. Yu, Synthesis of nitrogen-doped porous carbon nanofibers as an efficient electrode material for supercapacitors, ACS Nano 6 (2012) 7092–7102.
[38] X. Hong, K.S. Hui, Z. Zeng, K.N. Hui, L. Zhang, M. Mo, M. Li, Hierarchical nitrogen-doped porous carbon with high surface area derived from endothelium corneum gigeriae galli for high-performance supercapacitor, Electrochim. Acta 130 (2014) 464–469.
[39] Y.S. Yun, M.H. Park, S.J. Hong, M.E. Lee, Y.W. Park, H.J. Jin, Hierarchically porous carbon nanosheets from waste coffee grounds for supercapacitors, ACS Appl. Mater. Interfaces 7 (2015) 3684–3690.
[40] R. Liu, L. Wan, S. Liu, L. Pan, D. Wu, D. Zhao, An interface-induced co-assembly approach towards ordered mesoporous carbon/graphene aerogel for high-performance supercapacitors, Adv. Funct. Mater. 25 (2015) 526–533.
[41] T. Lin, I.-W. Chen, F. Liu, C. Yang, H. Bi, F. Xu, F. Huang, Nitrogen-doped

mesoporous carbon of extraordinary capacitance for electrochemical energy storage, Science 350 (2015) 1508–1513.
[42] C. Meng, C. Liu, L. Chen, C. Hu, S. Fan, Highly flexible and all-solid-state paperlike polymer supercapacitors, Nano Lett. 10 (2010) 4025–4031.
[43] X. Zhang, X. Wang, L. Jiang, H. Wu, C. Wu, J. Su, Effect of aqueous electrolytes on the electrochemical behaviors of supercapacitors based on hierarchically porous carbons, J. Power Sources 216 (2012) 290–296.
[44] B. Anothumakkool, A. Torris, S.N. Bhange, S.M. Unni, M.V. Badiger, S. Kurungot, Design of a high performance thin all-solid-state supercapacitor mimicking the active interface of its liquid-state counterpart, ACS Appl. Mater. Interfaces 5 (2013) 13397–13404.
[45] C. Masarapu, H.F. Zeng, K.H. Hung, B. Wei, Effect of temperature on the capacitance of carbon nanotube supercapacitors, ACS Nano 3 (2009) 2199–2206.